Momentum transport by neutrals: effect of kinetic coupling

J.T. Omotani[1], S.L. Newton[1,2], I. Pusztai[1], R. McDermott[3], M. Cavedon[3], T. Fülöp[1], the ASDEX Upgrade team and the EUROfusion MST1 Team*
[1]*Department of Physics, Chalmers University of Technology, 41296 Gothenburg, Sweden*
[2]*CCFE, Culham Science Centre, Abingdon, Oxon, OX14 3DB, UK*
[3]*Max-Planck-Institute for Plasma Physics, Boltzmannstr. 2, 85748 Garching, Germany*

Neutral particles play an important role in tokamak edge plasmas, influencing edge flow shear and the L-H transition. Through a series of charge exchange (CX) interactions, edge neutrals can result in a non-negligible population of hot neutrals inside the separatrix. We further investigate the effect of this population on the collisional transport of toroidal angular momentum, as it has been shown to be potentially significant even at low relative neutral density [1].

Codes conventionally used to model neutrals couple to a drifting-Maxwellian bulk plasma [2]. In contrast it has been shown analytically [3] that including the full, kinetic ion distribution function is crucial in cases with low external momentum input. Using a short mean free path (MFP) approximation for the neutrals, we have investigated this effect previously [1], and now compare the model to measurements in two ASDEX Upgrade (AUG) L-mode plasmas with different fuelling locations and no torque from neutral beam injection (NBI).

Short MFP neutrals

Solving the neutral kinetic equation in the short MFP limit allows the steady state, radial, collisional flux of toroidal angular momentum to be computed as [1, 4]

$$V'\left\langle R\hat{\boldsymbol{\zeta}}\cdot\boldsymbol{\Pi}_\mathrm{n}\cdot\nabla\psi\right\rangle = -\frac{1}{\nu_\mathrm{CX}}\frac{d}{d\psi}\left(V'\left\langle\frac{Rm_\mathrm{i}n_\mathrm{n}}{n_\mathrm{i}}\int d^3v\,(\hat{\boldsymbol{\zeta}}\cdot\boldsymbol{v})\,(\nabla\psi\cdot\boldsymbol{v})^2 f_\mathrm{i}\right\rangle\right). \tag{1}$$

We take as input the neoclassical distribution function f_i, calculated numerically by PERFECT [5] for shallow radial driving gradients (we do not consider H-mode), and the neutral density n_n. Subscripts n, i and B denote neutrals, main ions and boron impurity respectively, V is the volume enclosed by a flux surface, prime denotes the ψ-derivative, $2\pi\psi$ is the poloidal flux, R the major radius, $\hat{\boldsymbol{\zeta}} = \nabla\zeta/|\nabla\zeta|$ with ζ the toroidal angle, $\boldsymbol{\Pi}$ is the stress tensor, ν_CX the CX rate, m the mass, n the density, $\boldsymbol{v}$ the particle velocity, and $\langle\cdot\rangle$ denotes the flux surface average (FSA).

When the neutrals dominate momentum transport, they set the profile of the radial electric field E_r, and so the toroidal rotation, as we now show. Neglecting other momentum transport channels, $V'\left\langle R\hat{\boldsymbol{\zeta}}\cdot\boldsymbol{\Pi}_\mathrm{n}\cdot\nabla\psi\right\rangle = S_\mathrm{mom}(\psi)$ where S_mom is the total external momentum input within ψ. Integrating (1) radially inwards from the boundary ψ_b sets E_r, as first pointed out in [3],

$$X[f_\mathrm{i}] \equiv V'\left\langle\frac{Rm_\mathrm{i}n_\mathrm{n}}{n_\mathrm{i}}\int d^3v\,(\hat{\boldsymbol{\zeta}}\cdot\boldsymbol{v})\,(\nabla\psi\cdot\boldsymbol{v})^2 f_\mathrm{i}\right\rangle = -\int_{\psi_\mathrm{b}}^{\psi} d\psi'\,S_\mathrm{mom}\nu_\mathrm{CX} + C. \tag{2}$$

The integration constant C can be fixed by the measured boundary value of toroidal rotation of

*See H. Meyer et al, "Overview of progress in European Medium Sized Tokamaks towards an integrated plasma-edge/wall solution", accepted for publication in Nuclear Fusion.

any ion species as follows. In low flow ordering $V_{i\zeta} \ll v_{Ti}$, where v_{Ti} is the ion thermal velocity, the ion distribution at first order in the gyroradius expansion f_{i1} can be split into responses to the gradient of the lowest order Maxwellian component $f_{i0}(\psi)$ and to E_r: $f_{i1} = f_{i1}(E_r = 0) + f_{i1}^{(E)}$ and hence $X[f_i] = X[f_{i1}(E_r = 0)] + X[f_{i1}^{(E)}]$. The E_r response is rigid rotation [6], so $f_{i1}^{(E)} = m_i T_i^{-1} V^{(E)} \hat{\boldsymbol{\zeta}} \cdot \boldsymbol{v} f_{i0}$ where $V^{(E)} = -R\, d\Phi/d\psi$, with Φ the electrostatic potential, and $X[f_{i1}^{(E)}] = -V' \langle n_n R^4 B_p^2 \rangle T_i\, d\Phi/d\psi$. The difference between measured rotation at $\psi = \psi_b$ and simulated rotation for $E_r = 0$ gives the boundary value of $d\Phi/d\psi$. Thus eq. (2) evaluated at ψ_b sets C,

$$C = X[f_{i1}(E_r = 0), \psi_b] + V'(\psi_b) \langle n_n R^4 B_p^2 \rangle (\psi_b) T_i(\psi_b) \frac{d\Phi}{d\psi}(\psi_b) \tag{3}$$

and (2) gives $d\Phi/d\psi$, from which the required profiles of $V_{i\zeta}$ and $V_{B\zeta}$ can be predicted:

$$\frac{d\Phi}{d\psi} = -\frac{1}{V' \langle n_n R^4 B_p^2 \rangle T_i} \left(-\int_{\psi_b}^{\psi} d\psi'\, S_{mom} \nu_{CX} + C - X[f_{i1}(E_r = 0)] \right). \tag{4}$$

Changing the gas fuelling location alters the poloidal distribution of n_n, changing the poloidal weighting of the moment of f_i inside the FSA in (2) and of $R^4 {B_p}^2$ in the prefactor of (4).

Intrinsic rotation comparison

To test the predictions of the model above, two dedicated discharges were performed in AUG in which the variation in the edge rotation profiles with changes in the gas fuelling location was measured. These were nearly identical lower single null, L-mode plasmas with a low level of central electron cyclotron resonance heating (ECRH) to increase the length and stability of the discharge. They were fuelled either from a low field side (LFS) midplane or a lower divertor (div.) valve. The best match in the kinetic profiles exists between the midplane fuelled phase of discharge #33995 at $t = 3.0{-}4.5\,\mathrm{s}$ and the divertor fuelled phase of discharge #33997 from $t = 1.7{-}3.0\,\mathrm{s}$. The profiles from #33995, shown in Fig. 1, are used for all the modelling since those from #33997 are similar. Boron impurity rotation and temperature were measured using charge exchange recombination spectroscopy (CXRS) during NBI blips—we are restricted to low density plasmas to obtain sufficient CXRS signal. No change with fuelling location was observed in the rotation profiles, Fig. 2. This is consistent with the modelling, as we explain below.

Our neoclassical simulations take $Z_{eff} = 1.5$ due to a boron impurity in a deuterium bulk; varying Z_{eff} from 1.5 to 1.01 has a negligible effect on the results. Radial profiles of FSA neutral density are estimated using KN1D [7], taking plasma profiles from the outboard midplane. The absolute magnitude of the neutral density profile is difficult to determine experimentally, but does not affect the shape of the modelled profile. We take the molecular flux input of KN1D to be $2.1 \times 10^{21}\,\mathrm{molecules\,m^{-2}\,s^{-1}}$, giving the separatrix density $n_{n,sep} = 1.9 \times 10^{16}\,\mathrm{m^{-3}}$ and the modelled neutral density $n_n = 1.4 \times 10^{15}\,\mathrm{m^{-3}}$ at $\rho_{pol} = 0.96$, where $\rho_{pol} = \sqrt{\psi/\psi|_{sep}}$. The angular momentum flux through the neutrals (see (1), Fig. 3) is proportional to $n_{n,sep}$ whilst the rotation

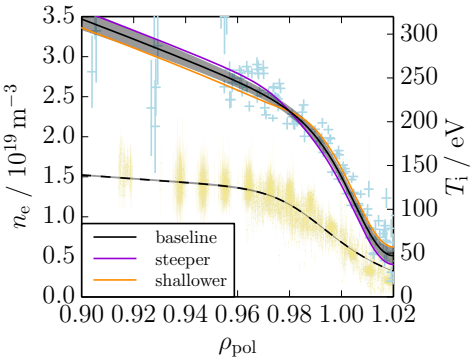

Figure 1: Fits (black) to T_i (solid) and n_e (dashed) profiles; fit uncertainty shown by grey shaded areas (≈line width for n_e). Markers show data points from #33995 for T_i (blue crosses) and n_e (yellow bars); vertical size gives the uncertainty. Steeper (purple) and shallower (orange) T_i profiles are used to test sensitivity.

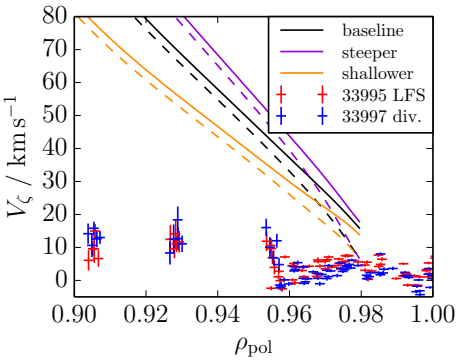

Figure 2: Comparison of predictions for main ion (solid lines) and B impurity (dashed lines) toroidal rotation for the profiles shown in Fig. 1 (baseline–black; steeper–purple; shallower–orange) to CXRS measurements (crosses, vertical bar shows experimental uncertainty) with LFS (red) and div. (blue) fuelling.

generated by the neutrals, Fig. 2, is independent of $n_{n,sep}$ as there is no external torque, $S_{mom} = 0$.

The rotation predicted by the model (4), taking a uniform poloidal profile for neutral density and the measured outboard midplane boundary condition $V_{B\zeta} = 5\,\mathrm{km}\,s^{-1}$ at $\rho_{pol} = 0.98$, is compared in Fig. 2 to measurements for both discharges. The sensitivity to variation in the T_i profile within fit uncertainties is also shown; forms of the steeper and shallower profiles were chosen as changing the gradient near where the boundary condition is set has the greatest impact on the rotation profile. In [8] the flux across the separatrix of neutrals from recycling was modelled in a similar L-mode as $357\,\mathrm{A} = 2.23 \times 10^{21}\,\mathrm{atoms\,s^{-1}}$. The gas fuelling rate in our experiment was $3.0 \times 10^{20}\,\mathrm{atoms\,s^{-1}}$ from the LFS valve ($2.4 \times 10^{20}\,\mathrm{atoms\,s^{-1}}$ from div.) and only a fraction will cross the separatrix. The ratio of these fluxes, 0.13, is larger than the ratio of number of puffed to background neutrals. We have therefore modelled poloidal profiles with the same FSA neutral densities, but where 10% of the neutrals are localized near the outboard midplane, inboard midplane or adjacent to the X-point, representing different fuelling locations, keeping the other 90% poloidally uniform, representing the background due to recycling. The response of the rotation to this change is smaller than the sensitivity to the T_i profile, and so is not plotted in Fig. 2.

The predicted rotation profiles are steeper than the measured ones, indicating that opposing transport mechanisms not included in this modelling are important. For example, the neoclassical momentum flux due to toroidal ripple has been shown to be significant, up to 0.5 N m for an AUG H-mode [9]. Residual stress (momentum flux excluding the part due to $V_{i\zeta}$) due to neutrals is calculated by taking the difference between the full neutral momentum flux (1) and that resulting from $f_{i1}^{(V)} \equiv m_i T_i^{-1} V_{i\zeta} \hat{\boldsymbol{\zeta}} \cdot \boldsymbol{\nu} f_{i0}$, with $V_{i\zeta}$ the simulated rotation, and is shown in Fig. 3. In the case of poloidally uniform neutrals the piece of the residual stress due to neutrals is the same order of magnitude as the momentum flux due to toroidal ripple in [9] and opposite in sign. It represents an inward flux of toroidal angular momentum, hence it drives the strong predicted

co-current rotation in Fig. 2. Fig. 3 also shows for comparison the same quantity from the various poloidal neutral profiles introduced above. The modest ratio $\sim 1.2-1.4$ between outboard and X-point profiles is consistent with the lack of variation in the measured rotation profiles, Fig. 2.

The limitations of the short MFP model should also be borne in mind: in this experiment, the scale length of the temperature $L_T = -(d \ln T_i/dr)^{-1}$ is shorter than the MFP for CX, $\lambda_{CX} = v_{Tn}/\nu_{CX}$, so the model, whilst available, cannot necessarily give a quantitatively accurate description.

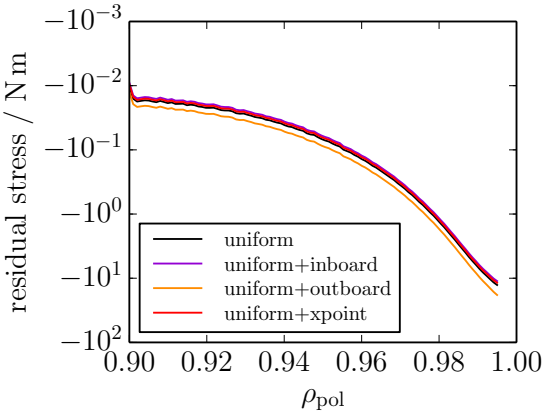

Figure 3: Piece of residual stress due to neutrals for different poloidal distributions of neutrals.

Summary

Neutrals couple to the non-Maxwellian as well as (drifting-)Maxwellian parts of the ion distribution function, producing a residual stress that can drive intrinsic rotation. Our modelling predicted a steeper slope of the toroidal rotation profile than observed in dedicated AUG discharges, suggesting the presence of opposing transport mechanisms. Losses from neutrals escaping to the wall which are not captured by the short MFP approximation, neoclassical torque from the toroidal ripple field or turbulent transport are all possibilities. Finally, we did not predict or observe a significant change in the measured rotation profiles when changing the gas fuelling location. This may be due to the modest fuelling possible in the low density discharges used.

Acknowledgements The authors would like to thank P. Schneider, E. Viezzer and E. Wolfrum for valuable discussions. This work was supported by the Framework grant for Strategic Energy Research (Dnr. 2014-5392) and the International Career Grant (Dnr. 330-2014-6313) from Vetenskapsrådet. This work has been carried out within the framework of the EUROfusion Consortium and has received funding from the Euratom research and training programme 2014-2018 under grant agreement No 633053. The views and opinions expressed herein do not necessarily reflect those of the European Commission.

References

[1] J. Omotani, I. Pusztai et al., *Nucl. Fusion*, **56**(12), 124002 (2016); J. Omotani, S. Newton et al., *Nucl. Fusion*, **57**(6), 066048 (2017).

[2] D. Reiter, M. Baelmans and P. Börner, *Fusion Sci. Technol.*, **47**(2), 172 (2005).

[3] P. Helander, T. Fülöp and P. J. Catto, *Phys. Plasmas*, **10**(11), 4396 (2003).

[4] P. J. Catto, P. Helander et al., *Phys. Plasmas*, **5**(11), 3961 (1998); T. Fülöp, P. J. Catto and P. Helander, *Phys. Plasmas*, **5**(9), 3398 (1998).

[5] M. Landreman, F. I. Parra et al., *Plasma Phys. Control. Fusion*, **56**(4), 045005 (2014).

[6] P. Helander et al., *Collisional transport in magnetized plasmas*, Cambridge University Press (2002).

[7] B. LaBombard, *KN1D: A 1-D space, 2-D velocity, kinetic transport algorithm for atomic and molecular hydrogen in an ionizing plasma*, PSFC, Massachusetts Institute of Technology (2001).

[8] T. Lunt, F. Reimold et al., *Plasma Phys. Control. Fusion*, **59**(5), 055016 (2017).

[9] A. F. Martitsch, S. V. Kasilov et al., *Plasma Phys. Control. Fusion*, **58**(7), 074007 (2016).